Beitr. Phys. Atmosph., August 1988, p. 204–218
0005–8173/88/03 0204–15 $ 3.00/0

Improvements of Simple Radiation Schemes for Mesoscale Models: a Case Study

F. Somieski[1], P. Koepke[2], K. T. Kriebel[1] and R. Meerkötter[2]

[1] DFVLR – Institut für Physik der Atmosphäre, D-8031 Oberpfaffenhofen, FRG
[2] Meteorologisches Institut, Universität München, Theresienstr. 37, D-8000 München 2, FRG

(Manuscript received October 1987, in final form May 1988)

Abstract

Reference radiation model results have been calculated to assess and improve simple parameterized radiation models which are applied in mesoscale circulation models. For cloud-free cases atmospheric heating rates (solar, terrestrial) and downward flux densities at the surface (direct solar, diffuse solar, terrestrial) are presented for several atmospheric and surface properties including different albedo and turbidity values, a ground inversion, and surface temperature deviations.

Reference model results are compared with results from the improved version of the Mahrer and Pielke (1977) radiation scheme and two other simple radiation models. Deviations generally are less than 5% for the total downward surface fluxes and less than 10 Wm^{-2} for the net fluxes at the surface. Concerning heating rates deviations are generally less than 20% or 1.5 K/d. In the layer between surface and 10 m height, larger deviations occur in the ground inversion case due to the strong vertical temperature gradients, if Sasamori's (1972) approximation is applied in the calculation of terrestrial heating rates.

Zusammenfassung

Verbesserung von einfachen Strahlungsparameterisierungen in Mesoscale-Modellen – Eine Fallstudie

Ergebnisse von Referenzstrahlungsmodellen werden berechnet zur Bewertung und Verbesserung einfacher, parameterisierter Strahlungsmodelle, die in mesoskaligen Zirkulationsmodellen verwendet werden. Für den wolkenfreien Fall werden Erwärmungsraten (im solaren und im terrestrischen Bereich) und die nach unten gerichteten Strahlungsflüsse am Boden (direkte solare, diffuse solare, terrestrische Strahlung) präsentiert und zwar für verschiedene Zustände der Atmosphäre und verschiedene Oberflächeneigenschaften, u.a. für verschiedene Albedo- und Trübungswerte, für Fälle mit Bodeninversion und Bodenoberflächentemperaturabweichung.

Die Ergebnisse der Referenzmodelle werden mit den Ergebnissen der verbesserten Version des Strahlungsmodells nach Mahrer und Pielke (1977) und mit zwei anderen einfachen Strahlungsmodellen verglichen. Die Abweichungen sind im allgemeinen kleiner als 5% für die nach unten gerichteten Gesamtstrahlungsflüsse am Boden und kleiner als 10 Wm^{-2} für die Nettostrahlungsflüsse am Boden. Die Abweichungen bei den Erwärmungsraten sind im allgemeinen kleiner als 20% oder 1.5 K/d. Im Bodeninversionsfall treten in der Schicht zwischen Boden und 10 m Höhe größere Abweichungen auf aufgrund der großen vertikalen Temperaturgradienten, wenn zur Berechnung der terrestrischen Erwärmungsraten die Approximation nach Sasamori (1972) verwendet wird.

1 Introduction

Realistic simulations of the diurnal cycle of thermally generated mesoscale atmospheric systems, as are seabreeze or mountain-valley-wind circulations, require a description of the radiative processes involved. To keep the computational effort reasonable, radiation schemes in mesoscale or other atmospheric circulation models are more or less parameterized compared to "exact" models, which numerically solve the equation of radiative transfer and perform a subsequent integration with respect to wavelength.

In order to quantify the accuracy of the radiation parameterization in general circulation models, the ICRCCM program (Intercomparison of Radiation Codes in Climate Models) was started. Results of terrestrial clear-sky radiation calculations (Luther and Fouquart, 1984) show an agreement concerning the downward surface flux densities of line-by-line models of about 5 Wm^{-2}, and of about 30 Wm^{-2} when parameterized models are compared. Unfortunately, special mesoscale aspects, as large temperature gradients near the surface, are not considered. Vogel and Wippermann (1982) compare different terrestrial radiation models

in the mesoscale application, but only models that are more or less parameterized. A number of radiation models in the solar spectral range are compared by Bird and Hulstrom (1981), but only direct irradiance is examined. Further simple solar radiation models are discussed and compared by Iqbal (1983). More complicated radiation models, based on so-called approximative methods, see e.g. Meador and Weaver (1980) or Bott and Zdunkowski (1983), have been developed for use in climate models. However, up to now there is no broad consent, what degree of complexity is necessary for application to mesoscale problems.

The purpose of this paper is to present improvements of the radiation scheme of the Mahrer and Pielke (1977) mesoscale model, which has been used in many places for a large number of mesoscale applications. The improvements are guided by comparing the model results with the corresponding results of "exact" radiation codes. These reference model results have been computed for different cloud-free atmospheric states and several surface properties especially focussed on mid-latitude mesoscale applications in elevated terrain. Of course, the set of cases is not complete in a sense that any possible configuration is taken into account. However, the cases cover a wide range of the natural variety in the mesoscale. The purpose is to show whether for these cases even simple radiation parameterizations yield results that are sufficiently accurate to be used in mesoscale models successfully.

Presently, there is no widely accepted "exact" radiation code to solve the equation of radiation transfer and to perform a wavelength integration in the solar spectral range. Therefore we use our own codes (Quenzel, 1978; Koepke and Kriebel, 1987) which are proved to give mathematically correct (Lenoble, 1977) and realistic results (Kriebel and Koepke, 1987). The terrestrial code (Graßl, 1978) used in this study is proved to give realistic results too (Luther and Fouquart, 1984).

Following a brief presentation of the reference radiation models used in this case study, we define the model input parameters concerning different atmospheric and surface properties. For comparison with parameterized radiation schemes the quantities of interest are the surface flux densities and the vertical profiles of the heating rates. Therefore reference surface flux densities are given in tables and atmospheric heating rates in graphical presentation. Then we present the radiation parameterization scheme of the Mahrer and Pielke (1977) model especially focussed on the improvements that have been made here together with two other simple radiation schemes. Finally the results of the model comparisons are listed and discussed with respect to the application in mesoscale circulation models.

2 Characteristics of the Reference Radiation Models

2a Reference Model for the Solar Spectral Range

Clear sky surface flux densities and heating rates in the solar spectral range (i.e. $\lambda \leqslant 3\,\mu m$) are computed in four steps: First, spectral radiances are calculated, second, integration over the wavelength is performed, third, the radiances are integrated to radiation flux densities and fourth, the heating rates are determined.

Spectral radiances $L(\vartheta_0, \vartheta, \phi)$ where ϑ_0, ϑ, ϕ denote the solar zenith angle, the zenith angle and the relative azimuth of a particular direction, respectively, are calculated by a successive-orders-of-scattering program (Quenzel, 1978) which accounts for all orders of scattering and allows for the use of spectral bidirectional reflection functions. The spectral scattering phase functions are calculated with a Mie computer program (Quenzel and Müller, 1978) which treats the particles as homogeneous spheres.

The integration over wavelength is done according to Koepke and Kriebel (1987), using spectral irradiances of the sun from Neckel and Labs (1981). The absorption of ozone is accounted for with absorption coefficients from Duetsch (1970). The absorption of water vapour, carbon dioxide and oxygen is handled by the exponential series method (e.g. Bakan et al., 1978). The values of the water vapour band absorption are calculated as in Moskalenko (1969) with coefficients from Koepke and Quenzel (1978) for the wavelengths below $1\,\mu m$ and from Moskalenko (1969) for the longer wavelengths. Aerosol single scattering albedo at $0.55\,\mu m$ is 0.89 and the corresponding fractional absorption increases with wavelength.

Upward directed radiances at the top of the atmosphere are calculated and both, upward and downward directed radiances at the bottom and at different layers within the atmosphere. These radiances are computed for 25 zenith and 80 azimuth angles and a direct integration over the hemisphere is performed to get the irradiance E (positive downward) and the radiant exitance M (positive upward).

The attenuated direct irradiance and the diffuse irradiance are calculated independently for all considered layers at different heights z. The atmospheric heating rates, represented by the temperature tendencies $\partial T/\partial t$, are calculated from the divergence of the

flux density $\Delta F/\Delta z$ with $\Delta F = E(z+\Delta z) - M(z+\Delta z) - (E(z) - M(z))$ as

$$\frac{\partial T}{\partial t} = \frac{1}{\rho c_p} \frac{\Delta F}{\Delta z} + C \qquad (1)$$

assuming a plane-parallel atmosphere where c_p is the heat capacity of the air at constant pressure and ρ is the air density. C symbolically describes the contribution of all non-radiative processes including dynamics and all diabatic processes other than radiation and is assumed to vanish in this context.

The spectral radiances are calculated with an accuracy of better than 1% as has been confirmed by comparison calculations (Lenoble, 1977). An even better accuracy is achieved with the integration to obtain the flux densities, since the integration is based on a sufficient number of data points. Comparison between values of the solar spectral irradiance measured in the visible and near infrared and those calculated with the coefficients used, show very good agreement (Cachorro et al., 1985). Water vapour band absorptions agree within 5% of the values derived from Yamamoto (1966) and Leupolt (1978). Since the water vapour absorption reduces the mean signal for the complete solar spectral range in the order of less than 15%, the remaining uncertainty is less than 1%. The coefficients of the exponential series to describe the water vapour absorption give the recovered band transmissions with an accuracy of better than 1% as well. The combination of these independent errors in the error propagation law gives a computational accuracy of 2% for the flux densities integrated over the solar spectral range. The systematic part of this error cancels in the differences used for the heating rates.

Essential information on the radiative properties of the atmosphere and the surface is contained in the spectral averages of the atmospheric turbidity and the surface albedo. Thus, these quantities are determined to allow for comparison of the reference model results with those from parameterized schemes. The surface albedo A for the complete solar range is given as

$$A(\vartheta_0) = M(z=0, \vartheta_0)/E(z=0, \vartheta_0) \qquad (2)$$

which can also be written as a wavelength average of the spectral albedos weighted with the spectral irradiance. The values of the surface albedo, which is used as an input parameter for the parameterized models, depend on the spectral and angular distribution of the irradiation, even for fixed spectral bidirectional reflection functions (e.g. Kriebel, 1979). Thus, A is a function both of the properties of the atmosphere and of the surface. The turbidity, expressed as the Linke turbidity factor T_L gives the total optical thickness of the atmosphere δ, including gas absorption and aerosol extinction, in multiples of the optical thickness δ_R of a pure Rayleigh atmosphere: $T_L = \delta/\delta_R$. It is calculated assuming the Lambert-Beer-law to be valid for the direct solar irradiance at the ground, attenuated by all atmospheric constituents, S and for S_R, which is the irradiance at the ground attenuated by molecules only. With E_0 the solar irradiance at the top of the atmosphere, the Linke turbidity factor T_L can be obtained from

$$T_L = \ln(S/E_0)/\ln(S_R/E_0) \qquad (3)$$

with the property that T_L depends slightly on the solar elevation angle in spite of constant atmospheric conditions, due to a saturation effect of the water vapour absorption bands.

2b Reference Model for the Terrestrial Spectral Range

In the terrestrial spectral range ($\lambda \geqslant 3\,\mu m$) the thermally emitted radiation cannot be neglected in the equation of radiative transfer as was done in the solar spectral range. On the other hand the azimuthal dependence of the radiances can be neglected because the source function is to a great extent determined by Planck's function. A solution for the equation of radiative transfer optimized to this situation is the Matrix-Operator-Theory. A rather detailed description of the method and the computer program used is given by Graßl (1978).

In the Matrix-Operator-Theory the vertically inhomogeneous atmosphere is divided into plane-parallel homogeneous sublayers. Each sublayer is characterized by its reflection, transmission and emission properties. A stepwise combination of such sublayers allows for radiative transfer calculations for any vertically inhomogeneous atmosphere. Calculated spectral radiance values are given at the surface and at the top of the atmosphere as well as between all homogeneous atmospheric sublayers. For the boundaries of each sublayer, upward and downward directed radiances are computed for five zenith angles θ corresponding to $\cos\theta = .1, .3, .5, .7, .9$. This has been shown to be sufficiently accurate for the hemispherical integration of these radiances to flux densities (Graßl, 1978). Vertical profiles of the spectral upward and downward directed fluxes are calculated and herewith the vertical profiles of the spectral net fluxes. After wavelength integration over the terrestrial spectral range the vertical profile of the heating rate is calculated according to eq. (1).

The terrestrial spectral range, which is considered from 100–2500 cm^{-1} (4–100 μm), is divided into

intervals which are mostly 100 cm^{-1} wide. In these rather broad spectral bands, the transmission functions of the absorbing gases water vapour H_2O, carbon dioxide CO_2 and ozone O_3 are evaluated with line data from Rothman (1978) and with a statistical band model after Goody (1964). The atmospheric transmission functions are approximated by exponential sums. Besides band absorption the model also accounts for a water vapour continuum absorption inside the spectral window region from 800–1200 cm^{-1}. Values for the water vapour continuum coefficients are taken from Graßl (1976). The accuracy of the flux densities is mainly limited by the use of the band model by Goody (1964). A computer code which is equivalent to the one used here, participated in the ICRCCM (Luther and Fouquart, 1984) and showed agreement to line by line codes in the 1–3% range for tropospherical flux densities. For small heating rates the error can become larger, because the differences of the flux densities used for heating rate calculations are very small compared to the flux densities themselves.

3 Input Data

The parameter sets which define the considered earth-atmosphere systems were chosen to match mesoscale applications where topographic features like different surface albedo and surface altitude or strong vertical temperature gradients, e.g. ground inversion, are of importance. Thus three horizontal surfaces are selected as the lower boundary conditions. They are characterized in the solar spectral range by measured spectral reflection functions and in the terrestrial spectral range by their typical emittances. The surface types are pasture land with an anisotropic reflection function (Kriebel, 1977, 1978) which shows a chlorophyll dependent increase at 0.7 μm and an emittance of 0.98 (Berényi, 1967; Blaxter, 1967); snow is used with an isotropic reflection function with a spectral distribution given by Kondratyev (1969) and an emittance of 0.98 (Berényi, 1967; Griggs, 1968); bare soil is taken with a reflection function obtained from Eaton and Dirmhirn (1979) and modified by Kriebel and Koepke (1987), with a spectral distribution given by Coulson and Reynolds (1971) and an emittance of 0.90 (Büttner and Kern, 1965; Sutherland and Bartholic, 1977). These surfaces are assumed to be at heights of 500 m and 2000 m above sea level. The temperature of the surfaces is taken to be equal to the air temperature of the US Standard Atmosphere in the same height above sea level. Additionally, deviations of the surface temperature from the air temperature of ± 20 K are assumed. Finally a surface temperature inversion is simulated where the surface is 15 K colder than the US Standard Atmosphere at this height and the air temperature increases logarithmically with height (assuming turbulent sensible heat exchange as main source for the air temperature deviation) and reaches the temperature of the US Standard Atmosphere in 200 m above the surface (Table 1). The reason for this is that in the cloud-free case the radiant flux densities at the surface and the heating rates near the surface are of importance. Especially the diurnal variations of the near surface terrestrial heating rates are mainly caused by the large temperature differences between the surface and the atmosphere.

The vertical temperature profile is taken from the US Standard Atmosphere (McClatchey et al., 1972). Also the vertical water vapour density profile is derived from it with the assumption that the relative humidity is constant with height with assumed relative humidi-

Table 1 Temperature deviation (ΔT) from Standard Atmosphere and specific humidity (q) *for ground inversion cases.* Index (e.g. 500/30) stands for surface altitude (500 m) and for relative humidity (30%) for the higher levels above the inversion. Humidity values in the last line refer to relative humidity.

height above ground surface m	ΔT K	$q_{500/30}$ 10^{-3}	$q_{500/70}$ 10^{-3}	$q_{2000/30}$ 10^{-3}	$q_{2000/70}$ 10^{-3}
0	−15.0	2.5	3.0	1.5	1.5
2	− 7.1	2.5	3.5	1.5	2.0
6	− 5.4	2.5	4.0	1.5	2.5
12	− 4.4	2.5	4.5	1.5	3.0
20	− 3.6	2.5	5.0	1.5	3.5
30	− 3.0	2.5	5.0	1.5	3.5
45	− 2.4	2.5	5.0	1.5	3.5
60	− 2.0	2.5	5.0	1.5	3.5
120	− 0.9	2.5	5.0	1.5	3.5
200 and higher	0.	30%	70%	30%	70%

ties of 30% and 70%. Humidity in the inversion cases is according to Table 1 with constant absolute humidity in the inversion layer for the 30% cases, but with reduced absolute humidity near the ground in the 70% cases in order to account for non-saturated air. A CO_2 content of 330 ppmV is taken and ozone is considered to be above the atmosphere with 0.3 atm-cm. In the solar spectral range the aerosol amount is varied with vertical profiles of the aerosol extinction coefficient at 0.55 μm given by McClatchey et al. (1971) and referred to as 'MC HAZY' and 'MC CLEAR' by Lenoble and Brogniez (1984). Slight modifications of the profiles below 6 km have been made to match the 'MC CLEAR' profile with $T_L(0.55) = 2$ and the 'MC HAZY' profile with $T_L(0.55) = 5$ at the level of both surface altitudes, where $T_L(0.55)$ is the spectral Linke turbidity factor at 0.55 μm wavelength at the surface. The aerosol type up to 12 km is continental background (Hänel and Bullrich, 1978) with the size distribution and the refractive index not changed with humidity. Above 12 km, stratospheric background aerosol after Lenoble and Brogniez (1984) is assumed. In the terrestrial spectral range, where aerosol absorption is less important, the aerosol particles are simply modelled after McClatchey et al. (1972) with 23 km ground visibility. To account for the daily course of the sun, in the solar spectral range all calculations are performed at three solar elevation angles of 12.5°, 32.5° and 57.5°.

4 Reference Results

4a Solar Spectral Range

Downward radiant flux densities at the bottom of the atmosphere are presented in Table 2 for the parameter combinations discussed in Chapter 3. The direct solar radiation S increases with increasing elevation of the sun and altitude of the surface and with decreasing turbidity and water vapour content. The diffuse radiation is given for different surface properties since this quantity, whose behaviour is opposite to that of the direct solar radiation, also depends on the albedo, due to multiple scattering processes. The values for the albedo of the three surface types also are shown, because these spectrally and spatially integrated quantities depend both on the variable spectral and variable spatial distribution of the illuminating global radiation, although the spectral bidirectional reflection functions are fixed for each of the investigated surface types. Additionally, the Linke turbidity factor T_L is presented in Table 2. It shall be reminded that T_L includes the combined effect on the atmospheric transmission of both aerosol particles and water vapour, in contrast to the spectral Linke turbidity factor $T_L(\lambda)$ which is defined as a measure of aerosol only and, hence, remains constant even if water vapour amount or solar elevation are changed. T_L increases with aerosol and water vapour amount. The decrease

Table 2 Solar downward radiant flux densities at the surface in Wm^{-2}, divided into the direct (S) and into the diffuse (D) part, albedo (A), total water vapour content (u) in $g\,cm^{-2}$, and Linke turbidity factor (T_L) from the reference model. Index 1 = pasture land, 2 = bare soil, 3 = snow.

elevation of the sun		12.5°				32.5°				57.5°			
spectral turbidity at 0.55 μm		2		5		2		5		2		5	
relative humidity in %		30	70	30	70	30	70	30	70	30	70	30	70
altitude of the surface = 500 m	S	133	125	68	63	475	456	339	324	831	805	661	638
	D_1	54	53	78	76	85	84	156	154	101	100	206	204
	D_2	55	54	79	77	89	88	165	162	106	105	219	216
	D_3	64	63	88	86	121	120	201	198	162	161	288	285
	A_1	0.25	0.24	0.25	0.24	0.21	0.21	0.22	0.21	0.20	0.19	0.20	0.20
	A_2	0.35	0.34	0.35	0.34	0.32	0.31	0.32	0.32	0.27	0.26	0.27	0.27
	A_3	0.74	0.75	0.72	0.73	0.75	0.75	0.74	0.75	0.75	0.76	0.74	0.75
	T_L	2.7	3.0	5.1	5.4	2.9	3.2	5.4	5.7	3.2	3.5	5.7	6.0
	u	0.70	1.63	0.70	1.63	0.70	1.63	0.70	1.63	0.70	1.63	0.70	1.63
altitude of the surface = 2000 m	S	149	141	83	78	504	489	379	366	868	848	715	697
	D_1	50	49	77	75	76	76	149	147	89	88	193	191
	D_2	51	50	78	76	80	79	154	152	94	93	199	197
	D_3	59	59	86	85	108	108	188	186	144	143	264	261
	A_1	0.25	0.24	0.25	0.24	0.21	0.21	0.22	0.21	0.20	0.20	0.20	0.20
	A_2	0.35	0.34	0.36	0.35	0.32	0.31	0.32	0.32	0.27	0.26	0.27	0.27
	A_3	0.73	0.74	0.72	0.73	0.75	0.75	0.74	0.74	0.75	0.75	0.74	0.75
	T_L	2.7	2.9	5.0	5.3	2.9	3.2	5.4	5.7	3.2	3.5	5.7	6.0
	u	0.35	0.81	0.35	0.81	0.35	0.81	0.35	0.81	0.35	0.81	0.35	0.81

of T_L with decreasing solar elevation in spite of unchanged atmospheric parameters is due to an increasing saturation of water vapour absorption bands with the effect that the relative influence of the pure Rayleigh atmosphere increases more rapidly than that of the atmosphere with all absorbers included.

Examples for heating rates as a function of the altitude above ground for three different solar elevations 12.5°, 32.5° and 57.5° are shown in Figure 1. The three different surfaces considered are bare soil, pasture land and snow as described in Chapter 3. They are assumed to be in 500 m above sea level. Two different states of the atmosphere are shown: dry atmosphere with low turbidity (f = 30%, $T_L(0.55)$ = 2) and wet atmosphere with high turbidity (f = 70%, $T_L(0.55)$ = 5). The flux densities have been computed at 0 m, 20 m, 60 m, 300 m, 600 m, 2000 m above ground level. Herefrom the heating rates have been calculated for each layer and a smoothed curve has been plotted through the centres of the layers.

The results for the surfaces in 2000 m above sea level are rather similar. The heating rates increase with the amount of available energy, i.e. solar elevation, and with the amount of absorbing material, i.e. turbidity and water vapour. The heating rates for the opposite combinations of turbidity and water vapour (f = 30%, $T_L(0.55)$ = 5; f = 70%, $T_L(0.55)$ = 2) are not shown because they lie in between the results given in Figure 1. The effect of water vapour is not as strong as that of the absorbing aerosol particles. The reason is that the water vapour absorbs within its bands only, while aerosol absorption takes place everywhere in the solar spectral range. Moreover, the water vapour absorption is easily saturated in parts of the bands which reduces

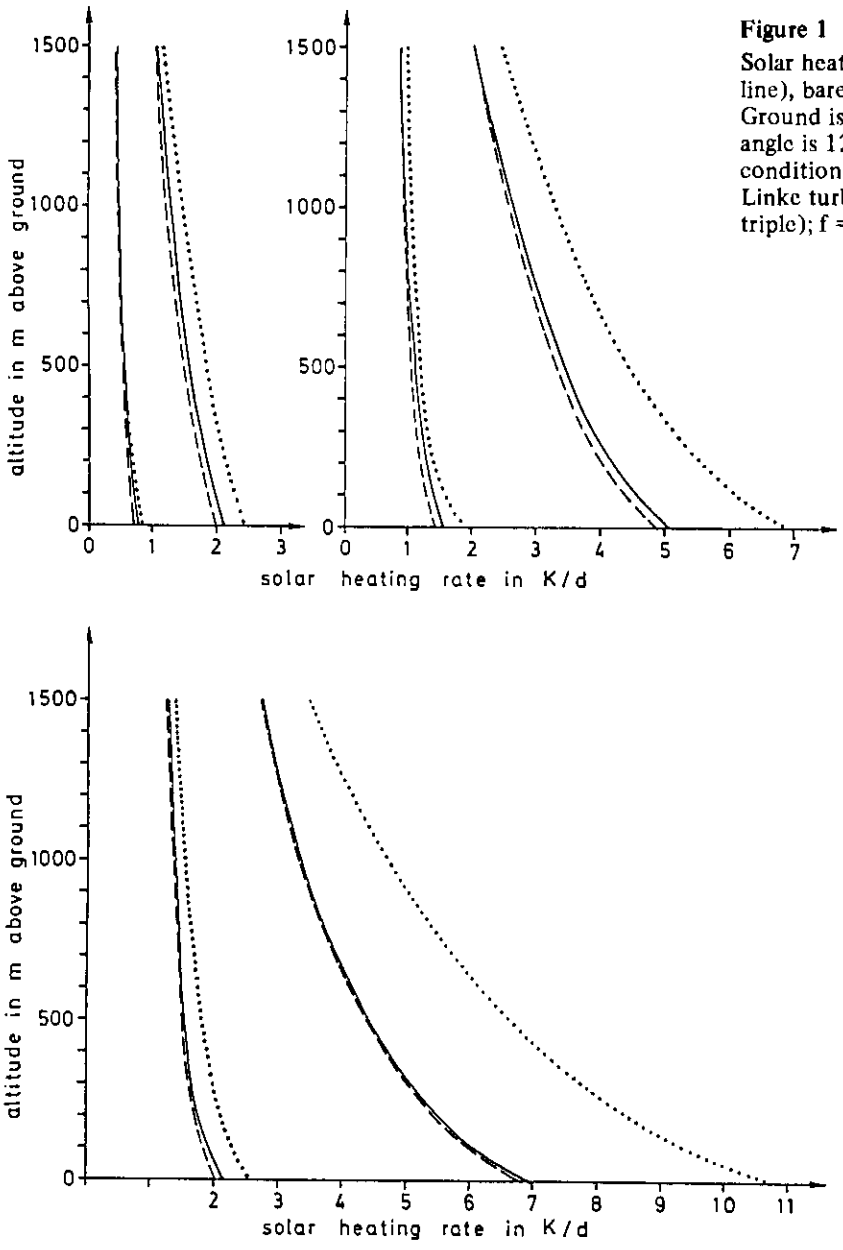

Figure 1
Solar heating rate profiles over pasture land (broken line), bare soil (solid line), and snow (dotted line). Ground is at 500 m above sea level. Solar elevation angle is 12.5° (a), 32.5° (b), 57.5° (c). Atmospheric conditions are relative humidity f = 30 %, spectral Linke turbidity factor at 0.55 μm T_L (0.55) = 2 (left triple); f = 70 %, T_L (0.55) = 5 (right triple).

their contribution to the heating rates especially at low solar elevation angles. An increase of the albedo increases the heating rates by generating additional multiple scattering processes in the atmosphere. Again this effect increases with turbidity, water vapour and solar elevation.

4b Terrestrial Spectral Range

Reference model surface fluxes, i.e. values of the downward directed flux densities and of the net flux densities at the surface are presented in Tables 3a and 3b. The downward directed flux densities at the surface vary with relative humidity and with surface altitude. The flux density values decrease by about 20% from 500 m to 2000 m altitude. Since absolute humidity depends on temperature, the atmospheric temperature profile above the high-altitude surface (in 2000 m) results in a lower water vapour content accompanied by reduced atmospheric emission temperatures which explains that downward fluxes are lower there.

Table 3a Terrestrial downward radiant flux densities in Wm^{-2} at the surface from the reference model.

	Standard Atmosphere		ground inversion	
altitude of the surface / relative humidity*	500 m	2000 m	500 m	2000 m
30%	244	196	234	189
70%	268	213	256	204

* For the exact near surface humidity profile in the ground inversion case see Table 1.

Comparing the downward flux densities for 30% and 70% relative humidity, Table 3a shows an increase of about 10% at 500 m versus an increase of 8% at 2000 m altitude. This small discrepancy is due to the fact that the variability of the water vapour content caused by variations of the relative humidity depends on the different atmospheric temperatures above both surfaces. In the case of the ground inversion, only emission temperatures within layers close to the surface are modified, whereas the absolute humidity remains nearly constant. Thus the downward directed flux density decreases only by about 4% as compared with the results of the unmodified temperature profile.

Table 3b presents model results of the terrestrial surface net flux density which is the sum of upward (negative sign) and downward directed flux density. According to the Stefan-Boltzmann-law $F = \epsilon\sigma T_s^4$ the upward flux density is linearly related to the surface emittance ϵ and reacts very sensitively to the surface temperature T_s. In the case of a ground inversion the absolute value of the net flux is strongly reduced due to the low surface temperature. Variations of the relative humidity influence the downward directed component (Table 3a). However, the reduction of the absolute net fluxes is not identical to the increase of the downward flux because the surface partly reflects the downward radiation. Surface net fluxes with the ground at 500 m and 2000 m, respectively, differ only little from each other. Decreasing surface emission tends to compensate the influence of reduced low level atmospheric humidity and temperature on the downward flux.

The vertical divergence of the net flux controls the heating or cooling rate. Thus an increase of the absolute value of the net flux (positive downward) with increasing height leads to a cooling of the atmospheric layers whereas a decrease heats the layers. Greatest flux divergences are computed for the cases with

Table 3b Terrestrial net flux densities at the surface in Wm^{-2} from the reference model.

	Standard Atmosphere, no surface temperature deviation				ground inversion	
emissivity	0.90		0.98		0.98	
altitude of the surface / relative humidity	500 m	2000 m	500 m	2000 m	500 m	2000 m
30%	−114	−114	−124	−124	−64	−68
70%	− 92	− 99	−100	−108	−42	−53

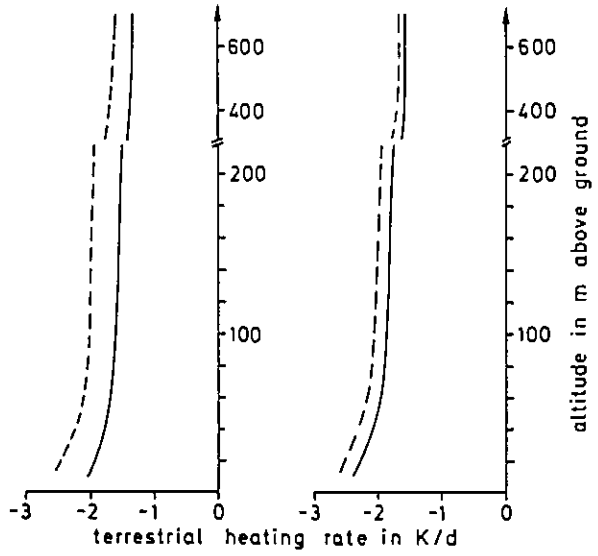

Figure 2 Terrestrial heating rates for the unmodified temperature profile with surface emissivity $\epsilon = 0.98$. Relative humidity is 30% (solid line) and 70% (broken line). Ground is at 500 m above sea level (left part), 2000 m above sea level (right part).

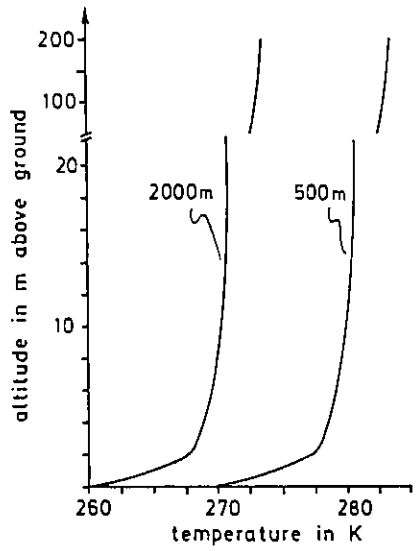

Figure 3a Temperature inversion for both ground surface altitudes.

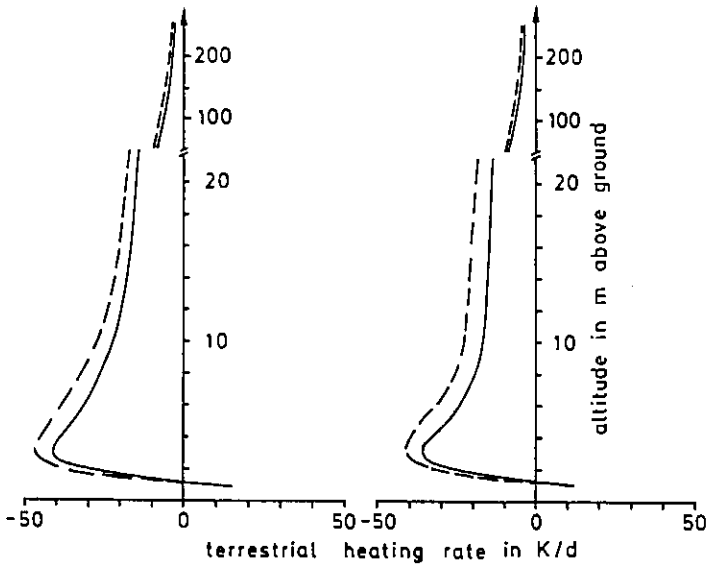

Figure 3b Terrestrial heating rates for the ground inversion case with surface emissivity $\epsilon = 0.98$. Relative humidity above the inversion is 30% (solid line) and 70% (broken line). Near surface humidity profiles are given in Table 1. Ground is at 500 m above sea level (left part), 2000 m above sea level (right part).

ground inversion and with surface temperature modifications. Looking firstly at the unmodified temperature profile in Figure 2, we note a cooling of each atmospheric layer due to an increasing net flux (absolute value) with height. The cooling rate itself, which is in the range of 1 to 3 K, decreases with altitude and would produce a ground inversion with time. A rather strong ground inversion, as constructed with regard to our model comparison (according to Table 1), is shown in Figure 3a. This temperature profile produces a heating within the first layer above the ground as shown in Figure 3b. The other layers above cool due to an enhanced net energy flux directed downwards to the colder surface layers caused by the increasing temperature gradient. This demonstrates that radiation flux divergence tends to smooth the sharp temperature gradient in our inversion case example. Figure 4 shows heating rate profiles resulting from surface temperature modifications of ± 20 K. An overheated surface produces a strong decrease of the net flux (absolute value) with height in the lower atmosphere accompanied with enhanced heating rates in the range of 70 to 120 K/d in the surface layer below 20 m. A colder surface (− 20 K), on the other side, results in a strong increase of the net flux above the surface. Consequently cooling rates of 60 to 100 K/d are computed for the layers close to the ground. Since the standard background terrestrial heating rate is about − 1.5 K/d, the profiles for the two cases are unsymmetrical to the zero-axis especially above 100 m.

Concerning vertical resolution close to the ground maximum resolution is 2 m in the inversion cases and 20 m for the other cases. (Effective resolution is still higher, due to internal generation of several sublayers assuming linearly varying atmospheric profiles.)

5 Original Mesoscale Radiation Parameterization Scheme

In a first step of model comparison, results from the original version of the Mahrer and Pielke (1977) mesoscale model radiation scheme had been compared

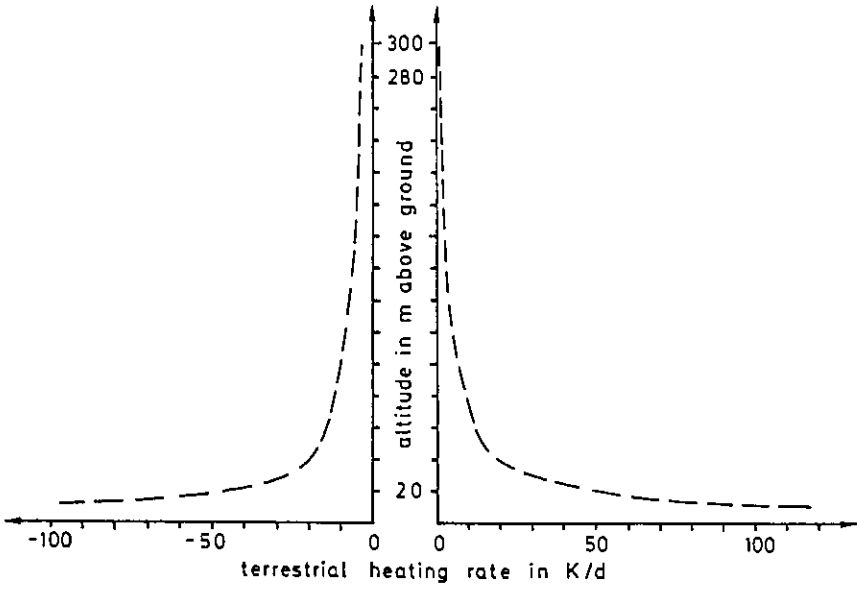

Figure 4
Terrestrial heating rates for surface temperature modifications (+ 20 K in the right part, − 20 K in the left part) with surface emissivity $\epsilon = 0.98$, relative humidity f = 70 %, and ground at 500 m above sea level.

with the reference model results. Mainly due to non-consideration of different albedo values and aerosol concentration in the original parameterization, deviations in the total solar downward flux densities were about 20% or 100 Wm^{-2}. Solar heating rates differed up to 100%. Terrestrial downward flux values were generally too high by about 10% or 30 Wm^{-2}, because of an incorrect upper boundary condition at the model top. Relative errors in the terrestrial net flux densities therefore became more than 100% in the cases with colder surface and inversion. Resulting differences in terrestrial heating rates amounted to 50%, in some cases much more, especially in the inversion case close to the ground.

After analyzing these large deviations, the parameterized scheme was modified, as described in the next chapter, and applied again. Only the results of this second approach will be discussed and compared to the reference model results.

6 Improvement of Mesoscale Model Radiation Schemes

Three parameterized radiation models are considered: an improved version of the Mahrer and Pielke (1977) model, a modified version of the Somieski (1978) model and the Angström-formula (Linke, 1970). The improvements consist of introducing additional transmissivities and functions to describe radiation physics not yet considered. These additional functions are taken from the literature cited or are designed to match the characteristic dependences shown by the reference model results. A final correction to reduce systematic differences is included. The main aspects of the improved model versions for clear-sky conditions, especially concerning the modifications with respect to the original models, are summarized in the following. A detailed description of the models including effects of slant surfaces and cloudiness, is given in Somieski (1987).

The radiation part of the Mahrer and Pielke (1977) mesoscale model is applied in a modified version (hereafter referred to as MMP-model):

In the solar spectral range the transmission functions and modification factors are connected by multiplication instead of addition. They account for the total (direct and diffuse) downward flux density E at the surface by further multiplication with μ, the sine of sun elevation, and the extraterrestrial solar flux density E_0

$$E = E_0 \mu T_E T_W T_D T_K f_A. \tag{4}$$

The transmission functions are T_E (Rayleigh scattering and absorption by permanent gases), T_W (absorption by water vapour), T_D (absorption by aerosol), T_K (systematic correction and attenuation due to aerosol scattering) and f_A (factor to account for different albedo values)

$$T_E = 0.485 + 0.515\,(1.041 - 0.16\,((0.000949\,p + 0.051)/\mu)^{1/2}) \tag{5}$$

$$T_W = 1 - 0.093\,(u/\mu)^{0.37} \tag{6}$$

$$T_D = \exp\left(-\frac{0.114}{\mu} \int_{\text{surface}}^{\text{top}} \tau(0.55)\,dz\right) \tag{7}$$

$$T_K = 0.97\,T_D \tag{8}$$

$$f_A = 1 + 0.1\,(A - 0.2) \tag{9}$$

with pressure p in hPa, total water vapour content u in g/cm^2, albedo A, aerosol extinction coefficient $\tau(0.55)$ at 0.55 μm. The transmission function T_E is according

to Atwater and Brown (1974). The function T_W used here is modified with respect to the original model according to Houghton in McDonald (1960) and the functions T_D, T_K, f_A have been additionally introduced. T_D and T_K are essentially according to Atwater and Brown (1974). The factor 0.114 is derived from the reference model calculations concerning wavelength integrated aerosol extinction coefficients and the factor 0.97 contains the final correction to reduce systematic differences between MMP-model and reference model results. The splitting of aerosol extinction into T_D and T_K is in order to compute the solar heating rates analytically. They are computed from the divergence of the downward flux due to absorption only, neglecting the absorbing part of T_E. A correcting factor f_r

$$f_r = 1 + A\frac{p}{p_G} \tag{10}$$

accounts for the effect of the upward flux due to surface reflection. For the solar heating rate $\partial T/\partial t$, which here is the temperature tendency only due to solar radiation absorption, we then obtain

$$\frac{\partial T}{\partial t} = \frac{1}{\rho c_p} E_0 f_r T_E T_K f_A T_D \times \left(0.114\, T_W \tau(0.55) - 0.0344\left(\frac{u}{\mu}\right)^{-0.63}\frac{\partial u}{\partial z}\right) \tag{11}$$

with the values of u and Δu (instead of ∂u) in g/cm^2.

The terrestrial part of the original scheme is applied with the modifications described in the following. A linear factor for pressure correction is additionally introduced into the calculation of total water vapour content and CO_2 content. In the CO_2 calculation the factor 0.415 is corrected to 0.26. The emissivities of water vapour and CO_2 are increased by a factor of 1.03 to achieve better agreement with the reference model. The emissivity at the model top (20 km) is changed to 0.15 in order to take into consideration a standard atmosphere situation above model top. Furthermore any value can now be assigned to the ground emissivity. In the calculation of the terrestrial heating rates, the approximation of Sasamori (1972) is applied and the surface reflection of the downward flux is taken into account.

In addition to the MMP-model two other simple models are used to calculate the downward flux densities at the surface:

For the downward terrestrial radiation flux density F we apply the Angström-formula (Linke, 1970) (hereafter Angström-model)

$$F = \sigma T_1^4 (0.79 - 0.174 \exp(-0.095\, e_1)) \tag{12}$$

as an example of an extremely simple parameterization, with σ Stefan-Boltzmann constant, e_1 water vapour pressure in hPa and T_1 air temperature, both in 2 m above the ground surface.

For the direct (S) and diffuse (D) solar radiation we use an improved version of the formulas originally given by Somieski (1978) (hereafter Somieski-model):

$$E = S + D \tag{13}$$

$$S = I\mu \tag{14}$$

$$D = I\mu f_A \frac{0.07\, T_L - 0.115}{\mu}\frac{p}{p_0} \tag{15}$$

with

$$f_A = 1 + 0.5\,(A - 0.2) \tag{16}$$

$$I = E_0 \exp\left(-\frac{T_L}{\mu} a_0 \frac{p}{p_0}\right) \tag{17}$$

$$a_0 = 0.040 + 0.065 \exp(-0.18/\mu) \tag{18}$$

where T_L is the Linke turbidity factor and $p_0 = 1013.25$ hPa. A value for the extraterrestrial solar radiation flux density E_0 of $1360\,Wm^{-2}$ is used here as well as in the MMP-model.

7 Comparison of the Results Obtained from the Reference Models and the Improved Radiation Parameterization Schemes

7a Surface Fluxes

The results concerning the comparison of surface flux densities are summarized in Table 4. They show the maximum deviations between the results obtained from the reference models and the parameterized models. Maximum deviations for the total downward flux densities are given in percent to show the relative accuracy of the radiation schemes. Absolute values for the net flux densities are given to assess the maximum

Table 4 Results of model comparison concerning downward and net fluxes at the surface: maximum deviation between parameterized model and reference model.

	MMP-model	Somieski-model
solar total downward solar net	3 % (snow: 5 %) 12 Wm^{-2}	6 % 15 Wm^{-2} *
	MMP-model	Angström-model
terrestrial downward terrestrial net	4 % 8 Wm^{-2}	7 % 14 Wm^{-2}

* Deviation up to 24 Wm^{-2} but with relative deviation less than 5 % for 4 cases out of a total of 72.

error of the effective, i.e. the absorbed energy at the surface. In the solar spectral range relative differences are the same for total downward and net flux densities. In the terrestrial spectral range this is valid for the absolute differences.

Comparing the solar fluxes at the surface, the deviations between reference model and MMP-model are less than 3% (less than 5% for snow surface) for the total downward flux densities. The solar net fluxes coincide within 12 Wm^{-2} or 5%. Compared with a 2% accuracy of the reference model itself, these differences are only slightly larger. The largest differences occur for the combination of the high albedo and the high turbidity cases, due to the inaccurate description of multiple scattering processes in the MMP-model.

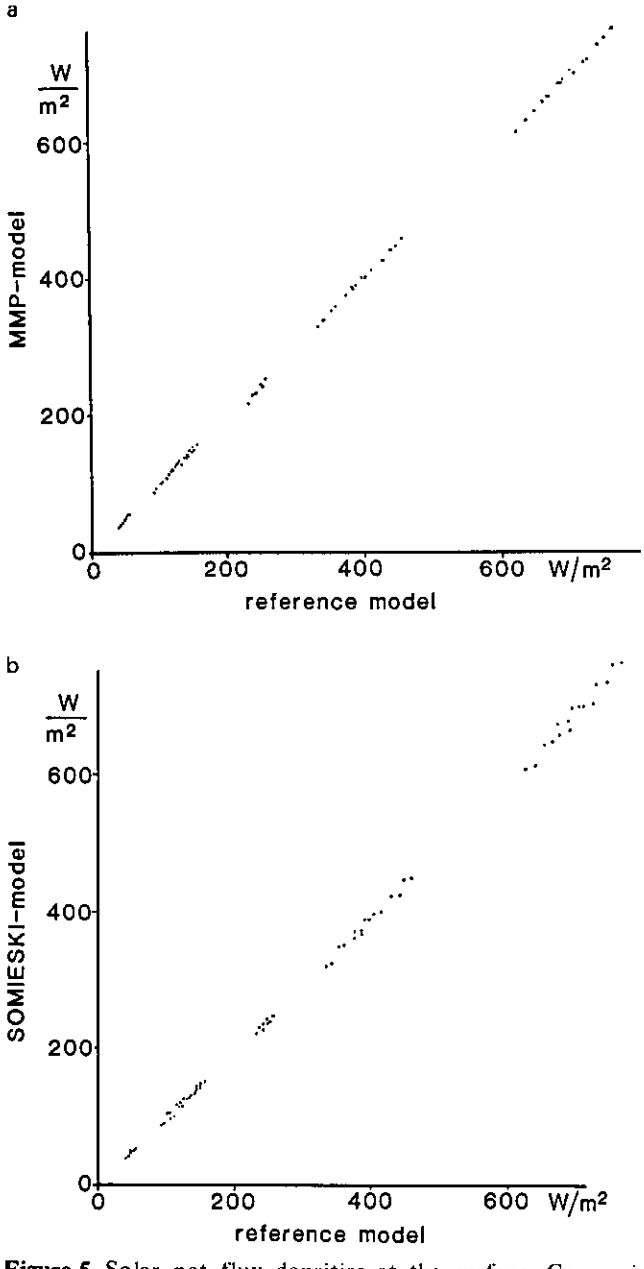

Figure 5 Solar net flux densities at the surface. Comparison of all 72 cases. MMP-model versus reference model (a), Somieski-model versus reference model (b).

Comparison of the net flux densities for all 72 cases is presented in Figure 5 for the MMP-model as well as for the Somieski-model. The deviations between the reference model and the Somieski-model are up to 6% for the total downward solar flux densities. These somewhat larger differences are due to a too simple calculation of diffuse radiation in the high albedo cases. These effects are apparent in Figure 6 which is presented as an example. Total downward solar radiation (i.e. global irradiance) and diffuse radiation are compared for the pasture land and snow surfaces in the 32.5° sun elevation case with the altitude of the ground surface at 2000 m. Those reference model cases, which differ only in relative humidity, are connected by lines to guide the eye. Results of the MMP-model are given in Figure 6 as well.

Figure 7 shows the comparison for all terrestrial downward surface flux densities with both the MMP-model and the Angström-model for relative humidities of 30% and 70% in each case, connected by lines to guide the eye again. The deviations between reference model and MMP-model are less than 4% for the downward fluxes. The absolute differences are less than 7 Wm^{-2} for the downward as well as for the net fluxes which are not shown in a figure. The largest deviations are in the 2000 m ground inversion case. The deviations of the Angström-model are only slightly larger, i.e. up to 7% for the downward terrestrial fluxes. Best

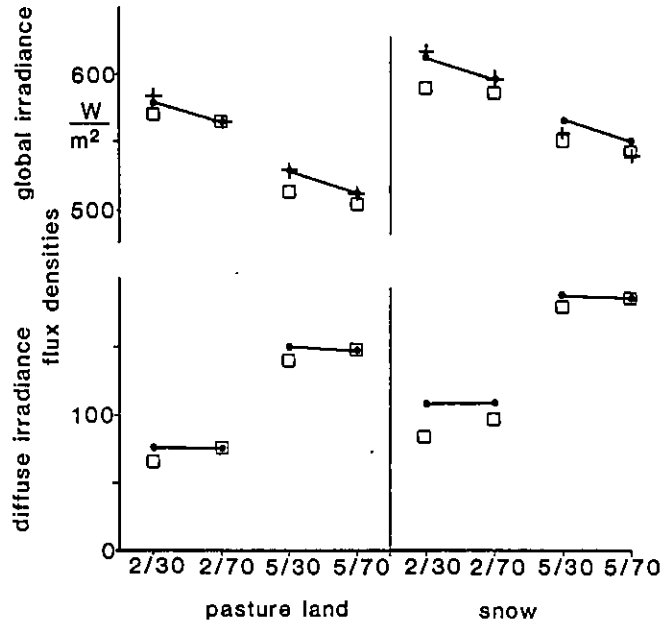

Figure 6 Solar downward flux densities at the surface for pasture land and snow surfaces. Altitude of the ground is 2000 m above sea level and sun elevation is 32.5°. The different cases are characterized by the spectral Linke turbidity factor at 0.55 μm / relative humidity of the atmosphere (e.g. 2/30). Full dots stand for the reference model, squares for the Somieski-model, crosses for the MMP-model (only global irradiance).

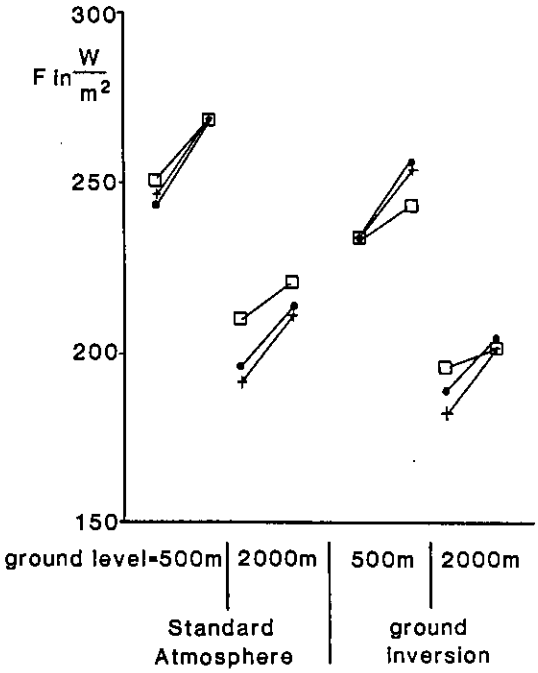

Figure 7 Terrestrial downward flux densities F at the surface for different atmospheres and altitudes of the ground. Full dots stand for the reference model, squares for the Angström-model, crosses for the MMP-model. Different relative humidity cases are connected by lines (symbol at the left end of the line corresponding to 30% relative humidity, right end to 70%). Ground inversion humidity profile is as in Table 1.

agreement is for the 500 m Standard Atmosphere case (Figure 7). The differences become larger for deviations of temperature from this "standard" case, or when there is an increase of absolute humidity with height as in the ground inversion cases with 70% relative humidity in the upper layers.

7b Heating Rates

The results concerning the comparison of heating rates are summarized in Table 5. The maximum deviations between the models in the different atmospheric layers are presented and in addition characteristic absolute values of heating rates are given to assess their relative importance.

In the solar spectral range the deviations of the heating rates between reference model and MMP-model are generally less than 20% or 1.5 K/d. For the case of high sun elevation angles together with high turbidity values the deviations are less than 30%. These somewhat larger differences can be seen, especially for the near surface values, in Figure 8 showing the comparison of the heating rates in the high turbidity case ($T_L(0.55) = 5$) with 70% relative humidity, pasture land surface and the altitude of the ground in 500 m.

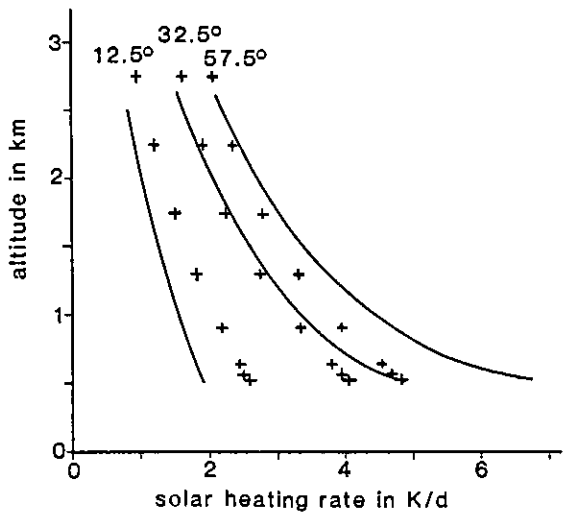

Figure 8 Solar heating rates for different sun elevation angles, pasture land, ground 500 m above sea level, relative humidity 70%, and high turbidity (spectral Linke turbidity factor at 0.55 μm is 5.0). Solid lines are for the reference model, crosses for the MMP-model.

Table 5 Results of model comparison concerning heating rates: maximum deviation between parameterized model (MMP-model) and reference models.

spectral range	layers above ground	deviation is less than	characteristic absolute values of heating rates are
solar	all layers	30% or 1.5 K/d	5 K/d**
terrestrial	0– 20 m	30%* or 1.1 K/d*	50 K/d
	20– 60 m	20% or 1.2 K/d	15 K/d
	60–200 m	20% or 1.5 K/d	5 K/d
	200–600 m	1.1 K/d	3 K/d
	>600 m	0.6 K/d	1.5 K/d

** Maximum values occur in the near surface layers
* In the layer 0–10 m much larger deviations are possible, if surface emissivity is 0.90 or in the ground inversion case.

For low sun elevation angles heating rates of the MMP-model are generally too large, for high sun elevation angles heating rates are generally too low. This is because the MMP-model only computes the total downward solar flux density and does not distinguish between direct and diffuse radiation. As a consequence, daily averages of the heating rate will have smaller differences due to compensation.

In the terrestrial spectral range the deviations are generally less than 20% or 1.5 K/d. For exact values of different atmospheric layers see Table 5. In the lowest layer (0–20 m) deviations are less than 30%. However, even larger deviations may occur in this layer in two cases: in the case with surface emissivity of 0.90 together with no surface temperature deviations (absolute values of heating rates are relatively low), and, more important, in the ground inversion cases. Calculations with high vertical resolution show that these deviations are largest very close to the ground and are significant only in the layer from 0 to 10 m. This effect is clearly shown in Figure 9 (left part) for one inversion case as an example. Sasamori's (1972) approximation of an isothermal atmosphere, with respect to the layer where the heating rate is calculated, causes large errors for extremely strong vertical temperature gradients as may occur close to the ground for inversion cases. In the layers above with less extreme temperature gradients and in the case of Standard Atmosphere with only surface temperature deviations (Figure 9, right part) the heating rates of the MMP-model agree well with those of the reference model.

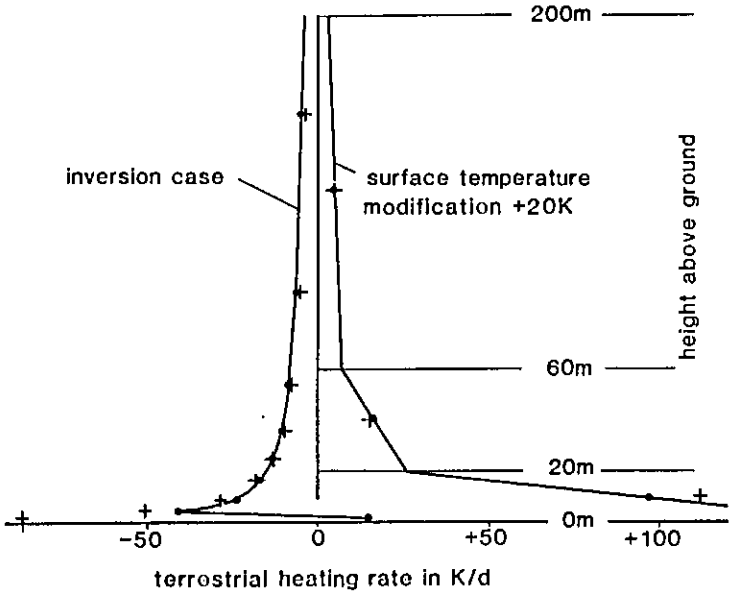

Figure 9 Terrestrial heating rates for relative humidity 30%, surface emissivity 0.98, ground 500 m above sea level. Solid lines and dots are for the reference model, crosses for the MMP-model.

8 Summary and Discussion with Respect to Mesoscale Applications

Many mesoscale model simulations require radiation parameterizations. Clear sky radiation surface fluxes and atmospheric heating rates, subdivided in the solar and the terrestrial part of the spectrum, are presented here for a range of well-defined atmospheric and surface properties including different albedo and turbidity values, ground inversion and surface temperature deviation cases. These different input parameter sets had been chosen according to midlatitude mesoscale application in elevated terrain. Sophisticated radiation models have been applied to obtain "reference" results. These results may be used by other modellers for comparison and model improvement.

Reference model results have been used here as a guide-line to improve simple parameterized radiation models. Comparing the results of the improved parameterized models with those of the reference models, we obtain very good agreement concerning surface fluxes with deviations generally less than 5% for the total downward flux densities and less than 10 Wm^{-2} for the net flux densities. Comparing atmospheric heating rates, deviations are generally less than 20% or less than 1.5 K/d. In the case of the ground inversion larger deviations occur in tbe layer 0–10 m concerning terrestrial heating rates when applying Sasamori's (1972) approximation of an isothermal atmosphere with respect to the layer of calculation.

In clear sky situations thermally sensitive mesoscale phenomena are primarily influenced by the sensible heat flux driven by surface net radiation. Mesoscale temperature tendencies due to radiation flux divergence are most important in the terrestrial range close to the ground. They have characteristic values of about 20 K/d in the lowest 100 m when there are pronounced temperature differences between ground surface and atmosphere. Inaccuracies concerning heating rates of about 2 K/d can be expected then to be of little importance of mesoscale circulations. It has been demonstrated here that simple, highly parameterized radiation models are able to compute surface radiation fluxes very accurately and terrestrial heating rates even with at least 20% accuracy. So these radiation models may be applied successfully for the simulation of many mesoscale phenomena influenced by radiation processes as mountain-valley winds, land-sea breeze, heat island, thermal influence on flow over and around mountains and through valleys.

However, one must bear in mind that the application of Sasamori's (1972) approximation may cause large errors, if terrestrial heating rates are required in the

lowest 10 m of the atmosphere, where large vertical temperature gradients may occur. For weak-wind, stably stratified ground inversion cases this approximation should be abandoned, if a detailed knowledge of the vertical profile of the atmospheric variables is required in the layer between surface and about 10 m height. When using parameterized models as those presented here in special cases, attention should be given to other, less significant inaccuracies. E.g., the surface net radiation is small, but still important, due to continuous low sun elevation in the artic regions (elevation angles less than 12.5° have not been discussed here), accurate solar heating rates are of importance for high turbidity values in industrial regions together with low sun elevation or high albedo values, or solar diffuse radiation is a matter for separate consideration (deviations are up to 24% in the Somieski-model, if only diffuse radiation fluxes are compared and the case of high albedo or small sun elevation angles is considered). Furthermore, radiation in tropical or arctic atmospheres and, more importantly, cloud effects parameterized in simple radiation schemes have not been discussed here, but this matter is currently being investigated.

In summary, even very simple parameterized radiation models yield rather accurate results, when results from reference radiation models for a number of atmospheric and surface parameter combinations are used for the improvement of the parameterized models. Therefore simple radiation schemes may be applied successfully for the simulation of many thermally influenced mesoscale processes. More complicated radiation models with high conceptional and computational expense appear to be necessary only for some special investigations.

Acknowledgements

We thank B. Dietrich for carrying out the computer calculations concerning the results of the reference model in the solar spectral range. Further thanks go to R. A. Pielke for making available a version of his mesoscale model and to H. Quenzel for stimulating our basic discussion on this work. G. Jacob is thanked for drawing of the figures and D. Janicke and M. Then for typing of parts of the manuscript. Part of the research was financed by the German Bundesministerium für Forschung und Technologie.

References

Atwater, M. A. and *P. S. Brown*, 1974: Numerical computations of the latitudinal variation of solar radiation for an atmosphere of varying opacity. J. Appl. Meteor., **13**, 289–297.

Bakan, S., *P. Koepke* and *H. Quenzel*, 1978: Radiation calculations in absorption bands: Comparison of exponential series and path length distribution – method. Beitr. Phys. Atmosph., **51**, 28–30.

Berényi, D., 1967: Mikroklima. Fischer Verlag, Stuttgart.

Bird, R. E. and *R. L. Hulstrom*, 1981: Review, evaluation, and improvement of direct irradiance models. J. Solar Energy Engineering, **103**, 182–192.

Blaxter, D. L., 1967: The energy metabolism of ruminants. Hutchinson, London.

Bott, A. and *W. Zdunkowski*, 1983: A fast solar radiation transfer code for application in climate models. Arch. Meteor. Geoph. Biocl., **B33**, 163–174.

Büttner, K. J. K. and *C. D. Kern*, 1965: The determination of infrared emissivities of terrestrial surfaces. J. Geophys. Res., **70**, 1329–1337.

Cachorro, V. E., *A. M. de Frutos* and *J. L. Casanova*, 1985: Comparison between various models of solar spectral irradiance and experimental data. Appl. Optics, **24**, 3249–3253.

Coulson, K. L. and *D. W. Reynolds*, 1971: The spectral reflectance of natural surfaces. J. Appl. Meteor., **10**, 1285–1295.

Dütsch, H. U., 1970: Absorptionskoeffizienten des Ozons. In: Linke, F. und F. Baur: Meteorologisches Taschenbuch, Band II, Akadem. Verlags Ges., Leipzig.

Eaton, F. D. and *I. Dirmhirn*, 1979: Reflected irradiance indicatrices of natural surfaces and their effect on albedo. Appl. Optics, **18**, 994–1008.

Goody, R. M., 1964: Atmospheric Radiation. Clarendon Press, Oxford.

Graßl, H., 1976: A new type of absorption in the atmospheric infrared window due to water vapour polymers. Beitr. Phys. Atmosph., **49**, 225–236.

Graßl, H., 1978: Strahlung in getrübten Atmosphären und in Wolken. Hamburger Geophys. Einzelschr. No. 37.

Griggs, M., 1968: Emissivities of natural surfaces in the 8 to 14 micron spectral region. J. Geophys. Res., **24**, 7545–7551.

Hänel, G. and *K. Bullrich*, 1978: Physico-chemical property models of tropospheric aerosol particles. Beitr. Phys. Atmosph., **51**, 129–138.

Iqbal, M., 1983: An introduction to solar radiation. Academic Press, New York.

Kondratyev, K. Y., 1969: Radiation in the atmosphere. Academic Press, New York.

Koepke, P., 1982: Meteosat-VIS-channel: Signal reduction due to atmospheric water vapor and ozone. Beitr. Phys. Atmosph., **55**, 358–369.

Koepke, P. and *H. Quenzel*, 1978: Water vapor: spectral transmission at wavelengths between 0.7 and 1 μm. Appl. Optics, 17, 2114–2118.

Koepke, P. and *K. T. Kriebel*, 1987: Improvements in the shortwave cloudfree radiation budget accuracy, Part I: Numerical study including surface anisotropy. J. Clim. Appl. Meteor., **26**, 374–395.

Kriebel, K. T. and *P. Koepke*, 1987: Improvements in the shortwave cloudfree radiation budget accuracy, Part II: Experimental study including mixed surface albedos. J. Clim. Appl. Meteor., **26**, 396–409.

Kriebel, K. T., 1977: Reflection properties of vegetated surfaces: tables of measured spectral biconical reflectance factors. Münchener Universitätsschriften, Meteor. Institut, Wiss. Mitt. Nr. 29, 82 pp.

Kriebel, K. T., 1978: Measured spectral bidirectional reflection properties of four vegetated surfaces. Appl. Optics, **17**, 253–259.

Kriebel, K. T., 1979: Albedo of vegetated surfaces: Its variability with differing irradiances. Rem. Sens. of Env., **8**, 283 - 290.

Lenoble, J. (Ed.), 1977: Standard procedures to compute atmospheric radiative transfer in a scattering atmosphere. Rep. No. 6, Radiation Comm., Int. Ass. Meteorol. and Atmos. Phys., Boulder, Colorado.

Lenoble, J. and *C. Brogniez*, 1984: A comparative review of radiation aerosol models. Beitr. Phys. Atmosph., **57**, 1–20.

Leupolt, A., 1978: Absorption of H_2O in the wavelength region 1–8 μm. Infrared Phys., **18**, 173–178.

Linke, F., 1970: Meteorologisches Taschenbuch. II. Band, Neue Ausgabe, Akademische Verlagsgesellschaft, Leipzig.

Luther, F. M. and *Y. Fouquart*, 1984: The intercomparison of radiation codes in climate models (ICRCCM) – longwave clear-sky calculations. Report of the ICRCCM meeting held in Frascati, Aug. 1984, World Climate Programme Report No. WCP-93, WMO, Geneva, 37 pp.

Mahrer, Y. and *R. A. Pielke*, 1977: A numerical study of the airflow over irregular terrain. Beitr. Phys. Atmosph., **50**, 98–113.

McClatchey, R. A., R. W. Fenn, J. E. A. Selby, F. E. Volz and *J. S. Garing*, 1971: Optical properties of the atmosphere. AFCRL Rep. No. 71-0279, Environmental Research Papers No. 354, Air Force Cambridge Res. Lab., Bedford, Mass.

McClatchey, R. A., R. W. Fenn, J. E. A. Selby, F. E. Volz and *J. S. Garing*, 1972: Optical properties of the atmosphere. AFCRL Rep. No. 72-0497, Air Force Cambridge Res. Lab., Bedford, Mass., (available as NTIS N7318412 from Nat. Techn. Inform. Serv., Springfield, Va.), 108 pp.

McDonald, J. E., 1960: Direct absorption of solar radiation by atmospheric water vapor. J. Meteor., **17**, 319–328.

Meador, W. E. and *W. R. Weaver*, 1980: Two stream approximations to radiative transfer in planetary atmospheres: A unified description of existing methods and a near improvement. J. Atmos. Sci., **37**, 630–643.

Moskalenko, N. L., 1969: The spectral transmission function in the bands of the water-vapor, O_3, N_2O and N_2 atmospheric components. Izv. Atmosp. Oceanic Phys., **5**, 1179–1190.

Neckel, H. and *D. Labs*, 1981: Improved data of solar spectral irradiance from 0.33 to 1.25 μm. Solar Phys., **74**, 231–242.

Quenzel, H., 1978: Computation of luminance and color distribution in the sky. In: Daylight illumination-color-contrast tables for full-form objects. Edited by M. R. Nagel, H. Quenzel, K. Kweta and R. Wendling, Academic Press, New York.

Quenzel, H. and *H. Müller*, 1978: Optical properties of single Mie particles. Münchener Universitätsschriften, Meteor. Institut, Wiss. Mitt. No. 34, 59 pp.

Rothman, L. S., 1978: Update of the AFGL atmospheric absorption line parameters compilation. Appl. Optics, **17**, 507.

Sasamori, T., 1972: A linear harmonic analysis of atmospheric motion with radiative dissipation. J. Meteor. Soc. Japan, **50**, 505–518.

Somieski, F., 1978: Ein Modell zur numerischen Simulation des Temperaturverhaltens eines Hauses. Diplomarbeit, Univ. München, 120 pp.

Somieski, F., 1987: Simulation der thermisch induzierten Gebirgswindzirkulation (Abschlußbericht). DFVLR, IB 553 9/87, Oberpfaffenhofen, 251 pp. (Available from DFVLR, Inst. Physik der Atmosphäre, D-8031 Oberpfaffenhofen.)

Sutherland, R. A. and *J. F. Bartholic*, 1977: Significance of vegetation in interpreting thermal radiation from terrestrial surface. J. Appl. Meteor., **16**, 759–763.

Vogel, B. and *F. Wippermann*, 1982: Untersuchung der Brauchbarkeit von Strahlungsmodellen mit unterschiedlichem Vereinfachungsgrad in numerischen Mesoscale Modellen. Vorhabensbericht Nr. 22 zum Vorhaben Mesoscale Simulationsmodell Oberrheingebiet, TH Darmstadt, Bonnenberg und Drescher, 67 pp.

Yamamoto, G., 1966: The effect of the atmosphere. In: N. Robinson (Ed.): Solar Radiation. Elsevier Publ. Comp., Amsterdam, 79–93.